

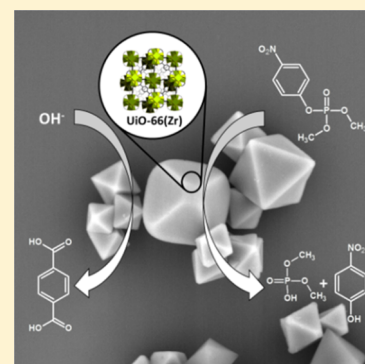
Zirconium Metal–Organic Framework UiO-66: Stability in an Aqueous Environment and Its Relevance for Organophosphate Degradation

 Daniel Bůžek,^{†,‡} Jan Demel,[†] and Kamil Lang^{*,†}
[†]Institute of Inorganic Chemistry of the Czech Academy of Sciences, 250 68 Řež, Czech Republic

[‡]Faculty of the Environment, Jan Evangelista Purkyně University, Králova Věšina 3132/7, 400 96 Ústí nad Labem, Czech Republic

Supporting Information

ABSTRACT: Zirconium-based metal–organic frameworks were recently investigated as catalysts for degradation of organophosphate toxic compounds, such as pesticides or chemical warfare agents. The most utilized UiO-66 is considered as a stable material for these applications in an aqueous environment. However, the presented results indicate that the properties of UiO-66 are changing considerably in aqueous media under common conditions used for organophosphate degradations, and therefore its catalytic activity is not related to the number of structural defects created during the material synthesis. We delineate the stability of UiO-66 in water of various pHs, the in situ formation of new catalytic sites, and the correlation of these two parameters with the degradation rate of a model organophosphate pollutant, dimethyl-4-nitrophenyl phosphate (methyl-paraoxon). The stability was quantified using high-performance liquid chromatography (HPLC) by measuring the amounts of leached terephthalic acid, the linker of UiO-66, and monocarboxylic acids, the modulators bound at UiO-66 defects. We demonstrate that the HPLC analysis is a more suitable method for metal–organic frameworks stability assessment than commonly used methods, e.g., powder X-ray diffraction, adsorption isotherms, or electron microscopy.



INTRODUCTION

Metal–organic frameworks (MOFs) are crystalline coordination polymers with an open framework containing potential voids. The structure is constructed from metal ions/clusters forming nodes, often referred as secondary building units (SBUs), which are linked together via coordination bonds with organic linkers, frequently di-, tri-, and tetraptopic carboxylic acids.^{1,2} Due to the variability of metals and linkers, MOFs provide a wide spectrum of structures and properties with high porosity and surface area often exceeding 1000 m² g⁻¹.³ Those properties make MOFs attractive candidates for gas storage and separation,^{4,5} catalysis,⁶ drug delivery,⁷ sensing,⁸ removal of hazardous compounds,^{9,10} light-harvesting,¹¹ and photocatalysis.¹²

Since the discovery, the zirconium-based family of MOFs have gained tremendous attention due to the high hydrothermal and chemical stability.^{13–15} The ideal structure of the most used UiO-66 is composed of Zr₆O₄(OH)₄¹²⁺ SBUs as 12-connected nodes linked together by terephthalic acids.¹⁶ Recent analyses using powder X-rays diffraction (XRD), scanning electron microscopy (SEM), nitrogen adsorption measurements, NMR, and thermogravimetric methods indicated that the structure of UiO-66 contains a number of defects (Scheme 1).^{15,17} Initially, missing-linker defects were predicted.^{18,19} However, strong evidence has been collected in last few years that missing-cluster defects prevail.^{20,21} The amount of these defects strongly depends on the conditions of

material syntheses. Similar to missing-linker defects, missing-cluster defects cause a deficiency of organic matter in the framework. Regardless the type of the defects, the missing-cluster/missing-linker dualism leads to the open-metal sites which provide catalytic activity toward organophosphate degradations.

Organophosphates or phosphate esters are a diverse group of compounds, which constitute not only essential biomolecules, e.g., ATP, DNA,²² but also highly toxic compounds such as pesticides (e.g., parathion, azinphos-methyl)²³ and nerve chemical warfare agents (sarin, soman, VX, etc.).^{24,25} Their toxic effect is based on inhibition of acetylcholinesterase during the neurotransmission leading to neuromuscular paralysis, followed by the respiration and heart arrest, and therefore they are extremely toxic toward insects and mammals.^{26,27} Due to their huge toxic risks, the development of fast and effective methods for organophosphate degradation is essential. In the past, several decontamination techniques were developed based on adsorption,²⁸ electrochemical²⁹ and photocatalytic degradations,³⁰ enzymatic biodegradation,³¹ and stoichiometric degradation with reactive sorbents.^{32,33} Despite the progress in the field, the degradation efficacy of contemporary materials still does not match the needs in protective applications against organophosphate toxins. In recent years,

Received: August 21, 2018

Scheme 1. Illustration of the UiO-66 Ideal (Non-Defect) Structure (Middle), and Missing-Cluster (Left) or Missing-Linker (Right) Defective Structures with Compensating Acetic and Formic Acids

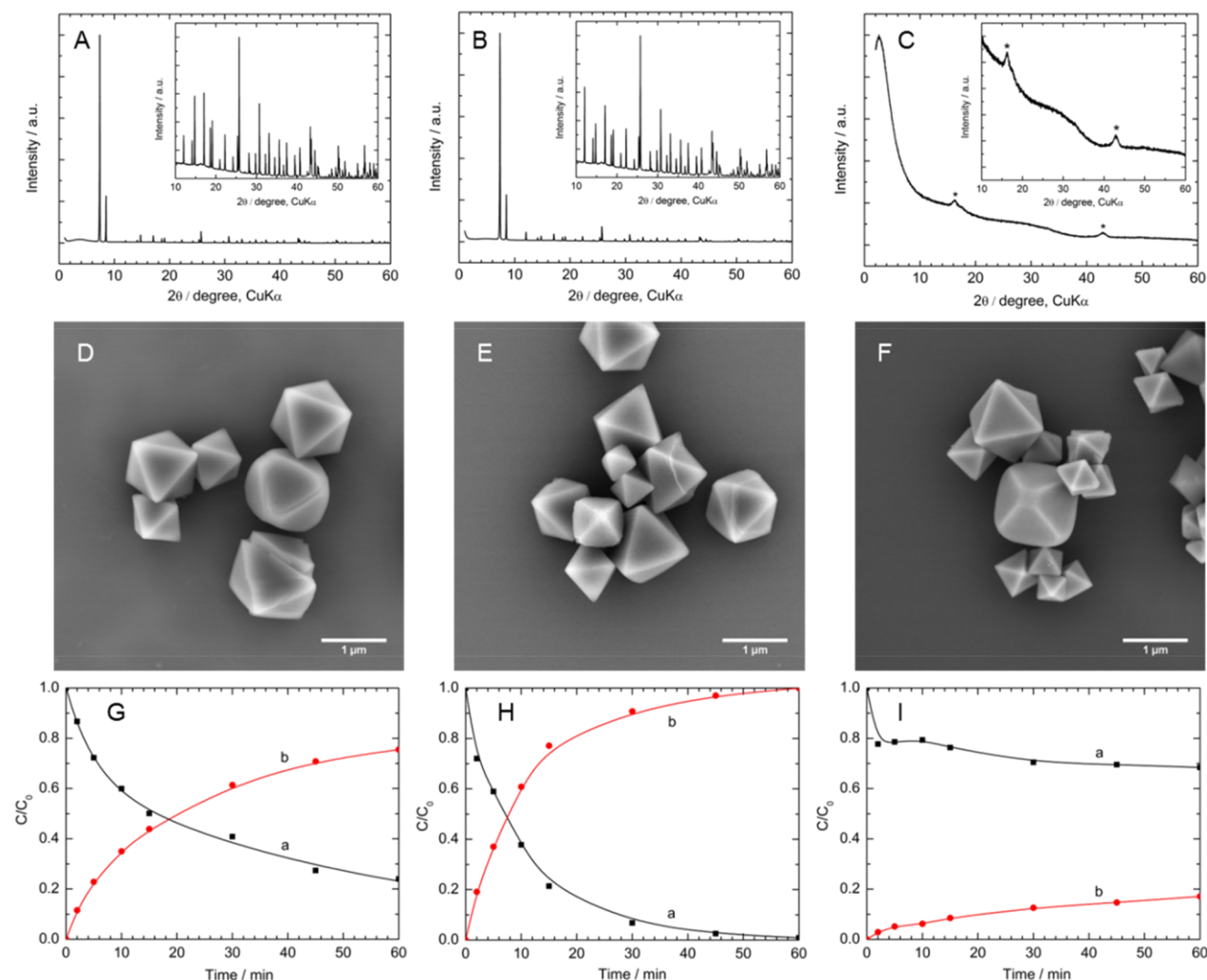
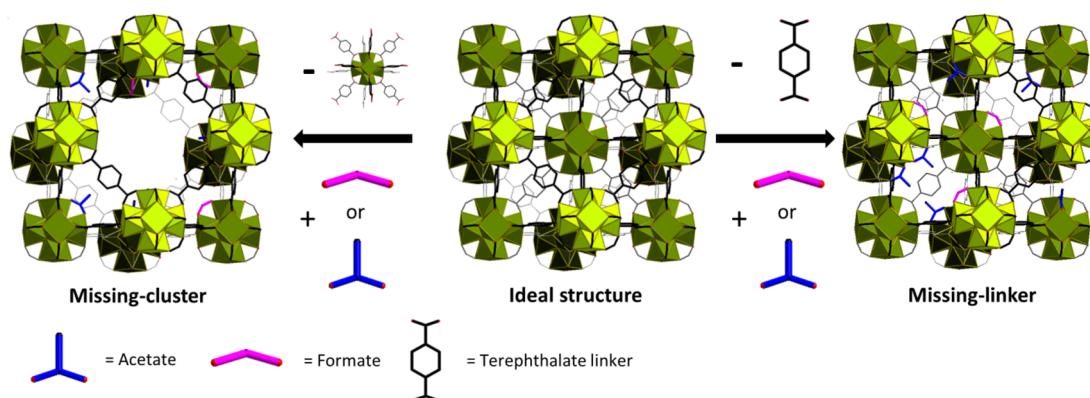


Figure 1. Properties of UiO-66. XRD patterns of as-prepared UiO-66 (A), and UiO-66 treated at pH 7.0 (B), and pH 11.0 (C) for 1 h. Inset: Magnified area 10–60° (2θ). The diffraction lines labeled by (*) belong to a Mylar foil used as a support. SEM images of as-prepared UiO-66 (D), and UiO-66 after 1 h treatment at pH 7.0 (E) and at pH 11.0 (F). Kinetics of dimethyl-4-nitrophenyl phosphate (DMNP) degradation (a) and 4-nitrophenol (4-NP) formation (b) at natural pH 3.8 (G), pH 7.0 (H), and pH 11.0 (I). All concentrations are determined with less than 5% error. XRD patterns (Figure S1), SEM images (Figure S2), N_2 adsorption isotherms (Figure S5), and kinetic curves (Figure S9) for all investigated pH values are presented in the [Supporting Information](#).

the zirconium-based family of MOFs, mainly UiO-66 and its derivatives, were studied as catalysts for organophosphate pesticide and nerve warfare agent degradation.^{34–39}

The organophosphate degradation by UiO-66 is associated with the reactivity of unsaturated sites on Lewis-acidic Zr^{IV} cations.^{34,36} Hupp et al.^{40,41} proposed that the catalytic

degradation in a narrow pH range is related to the coordinated $-\text{OH}_2$ molecules at the zirconium SBUs, which can be easily substituted by organophosphates. However, in light of recent results, it seems that instead of the terminal $-\text{OH}$ and $-\text{OH}_2$ ligands at the missing-linker defects, the terminal ligands are monocarboxylic acids, which were utilized as modulators during the syntheses or were formed by degradation of the solvent.^{20,21,42,43}

Here we report on the influence of pH on the degradation rate of a model organophosphate pollutant, dimethyl-4-nitrophenyl phosphate (DMNP), catalyzed by zirconium UiO-66. We studied the reaction in a broad pH range from pH 3.8 to 11.0 and thoroughly analyzed reaction mixtures using high-performance liquid chromatography (HPLC). This approach revealed a strong correlation between the amount of leached terephthalic acid from the UiO-66 structure and the catalytic activity. In light of the recent findings concerning defects in UiO-66,²⁰ our observation provides evidence that the reaction is initiated by zirconium-carboxylate bond breakage leading to the formation of open-metal sites, whose reactivity is responsible for the catalytic degradations.

RESULTS AND DISCUSSION

Synthesis and Characterization. UiO-66 was obtained by the solvothermal reaction of zirconium chloride with terephthalic acid in the presence of acetic acid as a modulator in 95 mol equiv to terephthalic acid. The resulting powder was then recovered from the synthesis solutions via centrifugation and washed with DMF and acetone. Water was not used for washing in order to eliminate all hydrolytic/leaching processes (see below). To confirm the identity of as-prepared UiO-66, we employed XRD, SEM, ^1H NMR, nitrogen adsorption, and thermogravimetric measurements.

The XRD pattern of as-prepared UiO-66 matches well with the pattern of microcrystalline UiO-66 (Figure 1, Figure S1).¹⁶ The only extra line is a broad diffraction at $1.9\text{--}6.5^\circ$, indicating the presence of structural defects (Figure S1).²⁰ SEM images show octahedral crystals with a broad size distribution varying from 0.5 to 2.0 μm (Figure 1, Figure S2). The BET surface area determined from N_2 adsorption isotherm is $1391\text{ m}^2\text{ g}^{-1}$, which is higher than that of the ideal (nondefect) UiO-66 structure (i.e., $1125\text{ m}^2\text{ g}^{-1}$).⁴⁴ (Table 1). The thermal behavior has features similar to those described in the literature (Figure S3).²⁰ The first broad endothermic peak between room temperature and $230\text{ }^\circ\text{C}$ with a weight loss of 10% corresponds to the release of surface and bound water molecules. An exothermic peak at approximately $400\text{ }^\circ\text{C}$ is

Table 1. Effect of pH on the Equilibrium Concentration of the Leached Terephthalate Linker and Surface Area after 1 h Treatment

pH	terephthalic acid/ mg L^{-1}	surface area/ $\text{m}^2\text{ g}^{-1}$
		1391 ^a
3.8	< LOD ^b	1331
5.5	1.2	1315
7.0	51	1285
8.5	114	1283
9.5	422	9
11.0	424	c

^aAs-prepared UiO-66. ^bLOD is the limit of detection (0.8 mg L^{-1}). ^cBelow detection limit.

accompanied by the release of water and carbon dioxide due to the thermal decomposition of the modulator anions. At this stage, UiO-66 is in the dehydroxylated form. The total thermal decomposition of UiO-66 starts at approximately $460\text{ }^\circ\text{C}$ and is connected with the combustion of the terephthalate linkers as indicated by CO_2 evolution. The thermogravimetric analysis gives a total weight loss of 55%.

In order to quantify the amount of monocarboxylate ligands, which compensate for the defects in the structure, UiO-66 was dissolved in 1 M NaOH/ D_2O followed by ^1H NMR measurements (Figure S4). The ^1H NMR spectrum shows typical peaks of formate (8.3 ppm), terephthalate (7.7 ppm), and acetate anions (1.7 ppm). In addition, traces of dimethylamine (2.1 ppm) were also identified. Formate anions and dimethylamine are the products of DMF thermal decomposition occurring during the solvothermal synthesis. The fact that both components were not removed by thorough washing of the material indicates that they are bonded to the UiO-66 framework; dimethylamine is probably ion-paired with the terminal terephthalate ligands and formate anions compensate for the defects similarly to intentionally added acetates. A terephthalate/acetate molar ratio of 1/0.18 ascertained from ^1H NMR measurement is in line with the reported results,²⁰ indicating that minimally 15% of zirconium coordination sites are occupied by acetates. A molar terephthalate/formate ratio of 1/0.13 is quite high probably due to relatively low activation temperature ($90\text{ }^\circ\text{C}$) used in our case. This result documents the high content of formates as an *in situ* produced modulator. In total, the measured terephthalate/monocarboxylate molar ratio is 1:0.31.

On the basis of the results described above, we conclude that our sample behaves very similarly to those analyzed by Lillerud et al.,²⁰ where the material is defective with predominant missing-cluster defects (reo phase) with compensating monocarboxylic acids bonded at the defective sites.

Stability of UiO-66 in Water and Its Dependence on pH. The assessment of the UiO-66 stability in aqueous solutions can enable rationalizing the catalytic activity at different pHs. Therefore, we first investigated the acid–base potentiometric titration of UiO-66 suspensions (Figure 2). The natural pH value of the suspensions is 3.8. The titration curve shows features similar to those described earlier.⁴⁵ The titration curve can be divided into three specific regions: (i) a steep pH increase from pH 3.8 to 8.5; (ii) a gradual increase from pH 8.5 to 9.5; (iii) finally, a rapid increase from pH 9.5

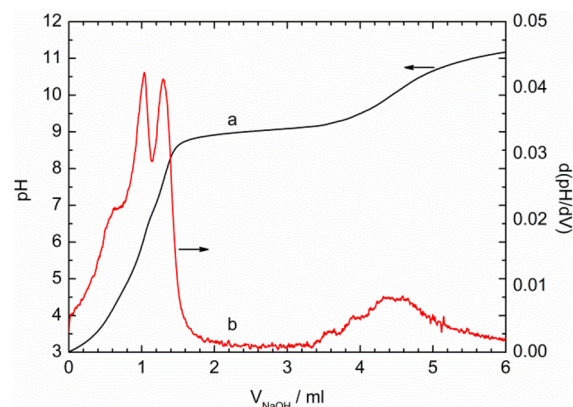


Figure 2. Acid–base titration curve of UiO-66 (a) and its first derivation (b).

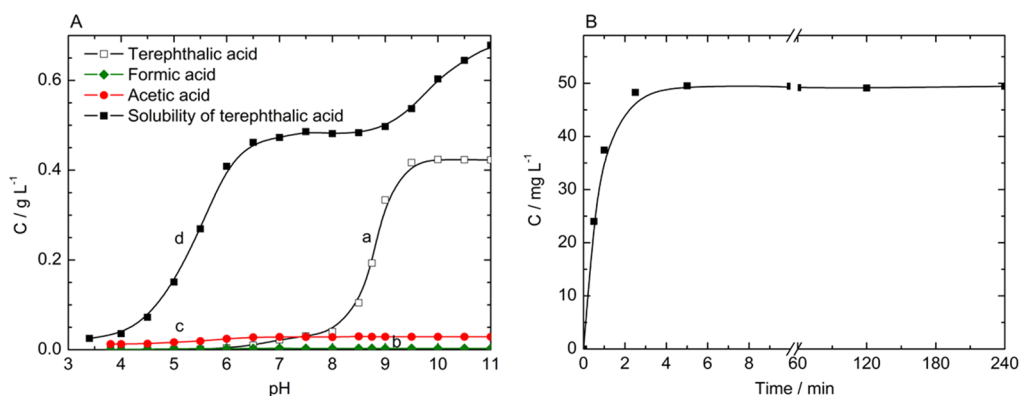


Figure 3. (A) Concentrations of terephthalic (a), acetic (b), and formic (c) acids leached immediately at different pHs from 50 mg of UiO-66 in 50 mL of water compared with the solubility of terephthalic acid in water (d). All concentrations are presented in Table S1. (B) Kinetics of the terephthalic acid release at pH 7.0; the equilibrium concentration is reached within 3 min.

up to more than 11.0. The titration curve has three equivalence points at pH 6.2 (1.04 mL 0.1 M NaOH), pH 7.9 (1.28 mL), and pH 10.1 (4.49 mL).

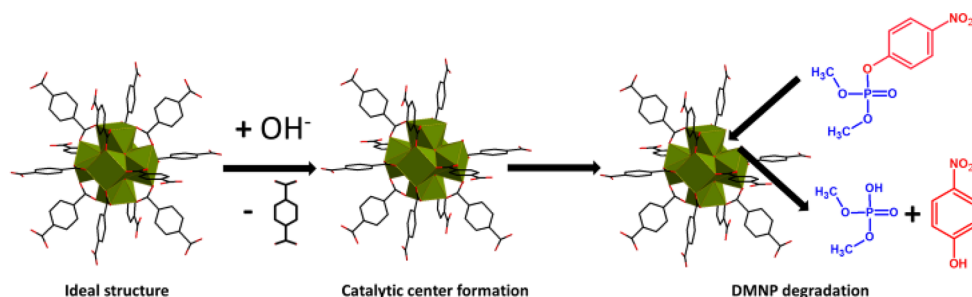
In order to unravel the structural changes of UiO-66 after contact with aqueous media of different pHs, UiO-66 was separated from the suspensions after 1 h at given pH and analyzed by powder XRD, nitrogen adsorption isotherms, and SEM. Using these standard techniques, the UiO-66 structure seems to remain nearly unchanged up to pH 8.5; however, the MOF structure completely collapses at pH 9.5 and above (Figure 1, Figure S1). The surface area of UiO-66 slightly decreases from 1391 m² g⁻¹ for the as-prepared material to 1283 m² g⁻¹ for the sample treated at pH 8.5, and finally, the treatment at greater pHs generates an abrupt drop (Table 1, Figure S5). Interestingly, SEM images do not indicate any morphological changes even at pH values above 9.5 (Figure 1, Figure S2), documenting the preservation of the particle morphology even after removal of the organic matter. Unfortunately, the broad size distribution of the original material masks a probable particle downsizing. To conclude, the used standard techniques indicate only minor structural changes of UiO-66 after the treatment at the pH between 3.8 and 8.5. The analysis of the SEM images is not conclusive even at greater pH values.

Thus, to track the changes to UiO-66 occurring in aqueous media at pH below 8.5, analytical methods of high sensitivity have to be utilized. In this context, the HPLC technique offers high accuracy for the analyses of leached terephthalic and monocarboxylic acids in concentrations down to approximately 1 ppm (1 mg L⁻¹) (Table 1, Table S1). During the course of the potentiometric titration, the concentrations of formic and acetic acids, measured immediately after reaching the given pH, gradually grow from 1 and 12 mg L⁻¹ up to approximately 3 and 29 mg L⁻¹ at pH 6.5, respectively, and then plateau at higher pHs (compare Figure 2 with Figure 3). On the other hand, terephthalic acid is not detected below pH 5.0; however, its immediate concentration is 22 mg L⁻¹ at pH 7.0, which is approximately 5% of the total linker content in as-prepared UiO-66 (Figure 3A, Table S1). At this point, we would like to note that the release is very fast, and the equilibrium concentration of terephthalic acid (approximately 13% of the linker content) is reached within 3 min (Figure 3B, Table 1). The concentration of released terephthalic acid steeply increases to more than 400 mg L⁻¹ at pHs above 9.5, indicating the total release of the linker (Figure 3A, Table 1,

Table S1). The abrupt release of terephthalic acid is evidently related to its pK_a values (pK_a 3.81 and 4.82), indicating its dissociation above pH 5.0, which sharply increases the solubility in water (Figure 3A). This massive release also correlates with the course of the titration curve, which shows the maximal buffer capacity in the region between pH 8.5 and 9.5. These findings can be further validated by the mass balance. The weight loss, attributed to the release of terephthalic and monocarboxylic acids at pH 11.0, is approximately 46%. The theoretical mass loss, calculated using the formula of ideal UiO-66 and simplifying the final product as ZrO₂, is approximately 45%, which matches the experimental result well. These data are also consistent with the thermogravimetric analysis described above. A total weight loss of 55%, from which approximately 10% is assigned to the water release, suggests that approximately 45% weight loss is connected with the combustion of the organic matter. The consistency of these results signifies that UiO-66 decomposes due to the complete release of the terephthalate linker at pH values above 9.5. In addition, the concentration of leached zirconium species to solutions is in all cases below the detection limit of the ICP-MS technique. Evidently, the hydrolysis of the Zr⁴⁺ species after the linker release is quite fast and leads to amorphous zirconium oxide hydroxide.

A terephthalate/acetate molar ratio of 1/0.19 measured by HPLC at pH above 9.5 is in very good agreement with the result of NMR-based dissolution analysis (i.e., 1/0.18). On the other hand, a terephthalate/formate molar ratio of 1/0.03 is much lower than the ratio of 1/0.13 obtained by the dissolution of UiO-66. The discrepancy originates in high concentration of NaOH needed for complete release of formic acid (i.e., 1 M NaOH). It follows from the repetition of the NMR-dissolution experiment using 0.1 M NaOH instead of 1 M NaOH. Under these conditions, a terephthalate/formate molar ratio was 1/0.04, i.e., coincident with the result of the leaching experiments measured using HPLC. It documents that only strongly basic conditions allow for the complete release of formate anions from hydrolyzed zirconium oxide-hydroxide. In contrast, the acetate ligands are easily substituted by the hydroxide ligands at common pHs.

With thus validated methodology, we decided to study the origin of the acidic pH of UiO-66 suspensions in water. To our surprise, 50 mg of UiO-66 suspended in 50 mL of deionized water released 12 mg L⁻¹ of acetic acid and less than 1 mg L⁻¹ of formic acid. No terephthalic acid was detected. Logically, we

Scheme 2. Formation of Open-Metal Sites at Zr(IV) SBUs of UiO-66 after the Release of the Terephthalate Linkers, and Coordinated Acetate and Formate Ligands^a


^aThese sites act as catalytic centers of DMNP degradation.

Table 2. Degradation of DMNP Catalyzed by UiO-66 at Different pHs^a

pH	conversion/%	$k_{\text{DMNP}}/\text{min}^{-1}$	$\tau_{1/2(\text{DMNP})}/\text{min}$	$k_{4\text{-NP}}/\text{min}^{-1}$	$\tau_{1/2(4\text{-NP})}/\text{min}$
3.8	76	0.035	20	0.032	22
5.0	75	0.032	22	0.030	23
5.5	80	0.039	20	0.034	18
6.0	81	0.049	14	0.039	18
7.0	100	0.105	7	0.094	7
8.5	100	0.116	6	0.104	7
9.5	37	n.a.	n.a.	n.a.	n.a.
11.0	17	n.a.	n.a.	n.a.	n.a.

^aConversion of DMNP is given after 60 min of the reaction; k_{DMNP} and $\tau_{1/2(\text{DMNP})}$ are the first-order rate constant and half-time of the DMNP degradation, respectively; $k_{4\text{-NP}}$ and $\tau_{1/2(4\text{-NP})}$ are the first-order rate constant and half-time of the 4-NP formation, respectively.

found the direct proportion between the suspended amount of UiO-66 and concentrations of the released monocarboxylic acids (Figure S6). At this point, we emphasize that as-prepared UiO-66 was thoroughly washed with DMF, the solvent in which both formic and acetic acids are well soluble, and therefore, the released acids were not occluded impurities within the UiO-66 structure. Evidently, the coordinated monocarboxylates, mainly acetates, are exchangeable with water molecules and released acid increases the acidity to pH 3.8.

In order to prove this assumption, as-prepared UiO-66 was treated with deionized water in five consecutive cycles (Figure S7). The concentrations of both acids gradually decrease as their supply in the structure is depleted. In concert with it, the natural pH value increases from pH 3.8 in the first cycle to pH 5.2 after the fifth cycle as the concentration of the released acetic acid decreased considerably. During this experiment, we did not observe any terephthalic acid leaching. On the other hand, five consecutive treatments of UiO-66 at pH 7.0 resulted in the repetitive leaching of terephthalic acid with decreasing equilibrium concentrations from one treatment to the other (Figure S8). On the basis of these results, we conclude that the leaching of the UiO-66 linker is a dynamic process, depending on the actual content of terephthalic acid in the sample and on the pH value. In addition, the equilibrium concentrations are reached quickly as documented by corresponding kinetics presented in Figure 3B. These findings point to the importance of the washing procedure on the resulting composition and properties of UiO-66.

Catalytic Activity of UiO-66 at Different pHs. As shown in the literature, the degradation of organophosphates is catalyzed by open-metal sites on Zr SBUs (Scheme 2).⁴¹ In order to correlate the stability of UiO-66 (see above) with the catalytic activity, we investigated the hydrolytic degradation of

DMNP leading to 4-NP and dimethyl phosphate at different pH values. Because dimethyl phosphate partially adsorbs onto UiO-66 (see the Supporting Information for details), we followed the course of the reaction by analyzing DMNP and 4-NP concentrations (Table 2, Figure 1, Figure S9). The reaction curves follow first-order kinetics, and the fitting to the monoexponential function gives corresponding rate constants and half-times. The blank reactions were evaluated in the absence of UiO-66. As expected, DMNP itself is stable in the broad range of pHs, and only a subtle conversion of approximately 3% at pH 11.0 after 60 min of the reaction was noticed.

In acidic pHs, the degradation kinetics of DMNP is quite slow with a half-time of 20 min at pH 3.8 and 14 min at pH 6.0. The half-times of the 4-NP formation are the same within the experimental error, which is expected for a simple monomolecular degradation mechanism (Scheme 2). As described above, this pH region is characterized by the predominant release of acetic acid from UiO-66, whereas the leaching of the terephthalate linker is a minor process. The release of acetic acid is accompanied by active sites formation catalyzing the organophosphate hydrolysis. At pHs between 7.0 and 8.5, the catalysis accelerates significantly, leading to the quantitative transformation of DMNP to 4-NP within 60 min with half-times of 7 min. These high reaction rates are evidently associated with the significant release of the terephthalate linker (Figure 3A), thus opening many new catalytic sites at the Zr₆ SBUs without the disruption of the UiO-66 structure (Scheme 2). Further increase of the pH above 9.5 leads to the deactivation of the catalyst within approximately 5 min and quite low conversions. Clearly, massive dissolution of the terephthalate linker from UiO-66 causes complete destruction of the UiO-66 structure, and the low conversions are due to a low catalytic activity of

amorphous zirconium oxide hydroxide,⁴⁶ formed by the decomposition of UiO-66.

The release of terephthalate linkers and monocarboxylate ligands at given pHs indicates the creation of coordinatively unsaturated sites *in situ* during the course of the reaction. In order to evaluate the effect of the number of created defects, UiO-66 was pretreated at pH 7.0 for 30 min, and its catalytic activity was investigated at lower pHs afterward (Figure S10). Clearly, the conversion of DMNP to 4-NP at pH 6.1 catalyzed by pretreated UiO-66 is comparable with that of as-prepared UiO-66 performed at pH 7.0. These results confirm the importance of the *in situ* defect formation for the catalytic reaction and suggest the ways for the improvement of the catalytic activity of UiO-66 at lower pHs, i.e., under conditions of higher stability of this material.

EXPERIMENTAL SECTION

Materials. Zirconium(IV) chloride (99.99% anhydrous), terephthalic acid, dimethyl-4-nitrophenyl phosphate (methyl-paraoxon, abbreviated hereafter as DMNP), 4-nitrophenol (abbreviated hereafter as 4-NP), methanol and acetonitrile (both for HPLC, gradient grade, Sigma-Aldrich), *N,N*-dimethylformamide (Penta, Czech Republic; abbreviated as DMF), acetic acid (99.8%), formic acid (98%), acetone, NaOH, HCl (35%) (all Lach-Ner, Czech Republic) were used as received.

Synthesis of UiO-66. UiO-66 was synthesized by the modified solvothermal procedure¹⁶ using a ZrCl₄/terephthalic acid molar ratio of 1:1. Zirconium chloride (106 mg, 0.455 mmol) was dissolved in DMF (20 mL) in a 40 mL Wheaton vial under sonication. Then, terephthalic acid (75.6 mg, 0.455 mmol) was added, followed by sonication to obtain a transparent solution. The solution was mixed with acetic acid (99.8%, 2.5 mL), and the vial was sealed. The crystallization was carried out in an oven at 120 °C for 24 h without stirring. The precipitate was separated by centrifugation (Hettich Rotina 35, 10 000 rpm, 5 min), washed four times with DMF and five times with acetone. The resulting white powder was air-dried overnight and activated at 90 °C under a dynamic vacuum for 24 h.

Instrumental Methods. Powder X-ray diffraction (XRD) was recorded using a PANalytical X'Pert PRO diffractometer in the transmission setup equipped with a conventional Cu X-ray tube (40 kV, 30 mA). Qualitative analysis was performed with the HighScorePlus software package (PANalytical, Almelo, The Netherlands, version 3.0) and the JCPDS PDF-2 database.⁴⁷ The porosity was probed by measuring nitrogen adsorption isotherms at 77 K using a Belsorp max II instrument (Microtrac Bel). Prior to the adsorption experiments, the samples were evacuated at 90 °C for at least 24 h. The surface area was determined using the Brunauer–Emmett–Teller (BET) method. High-resolution scanning electron microscopy (SEM) was performed using a FEI Nova NanoSEM equipped with a circular backscatter detector in the backscattered electron mode. An accelerating voltage was set to 5 or 10 kV. UiO-66 was suspended in acetone in an ultrasonic bath and deposited onto a silicon wafer chip, and the deposit was air-dried overnight.

The acid–base titration of UiO-66 was performed using an automatic Titrator 794 Basic Titrimo (Metrohm, Switzerland). 50 mg of UiO-66 was transferred to a beaker and 50 mL of water was added, followed by 15 min sonication leading to the milky-like suspension. The pH was adjusted to 3.0 using 0.1 M HCl, and the stirred suspension was titrated by 0.1 M NaOH with a rate of 0.04 mL min⁻¹ up to pH 11.3. The titration experiments were repeated three times with excellent reproducibility.

The concentrations of DMNP and 4-NP were measured using an HPLC-DAD DIONEX UltiMate 3000 instrument equipped with a diode array detector, 20 μL sampling loop, and a Kinetex 2.6 μm C18 column (Phenomenex, USA, 50 mm × 3 mm). Methanol/water was used as a mobile phase (0.5 mL min⁻¹, both solvents contain 0.1% HCOOH) with a gradient starting from 40/60 to 95/5 (v/v). The time of analysis was set to 5 min followed by equilibration for 2 min,

and the signals were collected at 272 and 300 nm for DMNP and 4-NP, respectively. Terephthalic acid was analyzed on a Hydrosphere 5 μm C18 column (YMC HPLC COLUMN, Japan, 150 mm × 4.6 mm) under isocratic elution (1 mL min⁻¹) with a 30/70 (v/v) acetonitrile/water/0.1% HCOOH mobile phase. The time of analysis was set to 5 min, and the signal was collected at 240 nm. Formic and acetic acids were quantified using a Synergi 4 μm polar-RP 80 A column (Phenomenex, USA, 100 mm × 4.6 mm) with a water/0.1% HCl mobile phase (0.5 mL min⁻¹). The time of the analysis was set to 5 min followed by equilibration for 5 min, and the signals were collected at 210 nm. The concentrations of all compounds were evaluated using the calibration curve method. The concentration of leached zirconium was measured on an ICP-MS Agilent 7700 equipped with an argon burner, ion optics, collision reaction ORS 3 cell, and hyperbolic quadrupole mass analyzer with a DDEM detector. The samples (1 mL, pH 3.8–11.0, filtration using 0.1 μm microfilters) were measured under the helium and no-gas mode, and the detector was set on the mass of 90 and 91 for ⁹⁰Zr and ⁹¹Zr, respectively.

¹H NMR spectra were measured using a JEOL 600 MHz NMR spectrometer. The chemical shifts are referenced to the residual ¹H signal of D₂O. Thermal analyses were carried out on a Setaram SETSYS Evolution-16-MS instrument coupled with a mass spectrometer. The measurements were performed in synthetic air (30 mL min⁻¹) from 20 to 800 °C with a heating rate of 5 °C min⁻¹.

Stability Testing of UiO-66. Concentrations of terephthalic, formic, and acetic acid released from UiO-66 in water were determined at a natural pH value of 3.8 and at pHs between 4.0 and 11.0 with a step of 0.5. The procedure was as follows: 50 mg of UiO-66 was mixed with 50 mL of water, shortly sonicated, and the pH values were adjusted by adding 0.1 M NaOH using the automatic Titrator 794 Basic Titrimo (Metrohm, Switzerland). Aliquots of 0.2 mL were taken immediately after reaching the respective pH values, filtered through Whatman microfilters (0.2 μm, PTFE), and analyzed by HPLC as described above. The immediate solubility of terephthalic acid was measured in the stirred dispersion of 50 mg of terephthalic acid in 50 mL of water using the same procedure. The equilibrium concentrations of terephthalic acid at given pH values were measured in the dispersions after 1 h of stirring. The kinetics of terephthalic acid release was measured at pH 7.0 with sampling from 0.5 to 240 min. All presented concentrations are the mean values of three independent experiments. The standard deviations are lower than 10%.

Liquid ¹H NMR spectra were measured after the dissolution of 20 mg of UiO-66 in 0.8 mL of 1 M NaOH in D₂O. UiO-66 was dissolved overnight at room temperature similar to the procedure developed by Lillerud et al.²⁰

Degradation of DMNP at Different pHs. In a typical experiment, 2 mg of activated UiO-66 (24 h, 90 °C under a dynamic vacuum) was mixed with 1.75 mL of water in a 4 mL vial and sonicated to form a turbid suspension. In degradation experiments at the natural pH (pH 3.8), 0.25 mL of 8 mM DMNP aqueous solution was added. The pH was adjusted by consecutive additions of 0.1 M NaOH to 5.0, 5.5, 6.0, 7.0, 8.5, 9.5, and 11.0 using the automatic Titrator 794 Basic Titrimo followed by the addition of 8 mM DMNP. The initial concentration of DMNP was 1 mM. During the reaction, the pH values were kept constant using the automatic titrator. The reaction was performed under stirring at room temperature; 50 μL samples were taken at regular intervals (2, 5, 10, 15, 30, 45, and 60 min) and diluted with 1 mL of 0.1% HCOOH to stop the reaction. Finally, the samples were filtered using a 0.2 μm PTFE Whatmann microfilter and analyzed by HPLC. Pretreated UiO-66 was prepared by the mixing of 2 mg of as-prepared UiO-66 with water adjusted to pH 7.0. After 30 min of stirring, solid UiO-66 was separated by centrifugation and washed twice with water until the absence of terephthalic acid in the solution. Then, the solid was used in degradation experiments as described above without pH adjustment. Blank experiments were performed by the analogous procedure in the absence of UiO-66. The presented results are the average values of three independent experiments. In all cases, the standard deviations are lower than 5%.

Structural Changes of UiO-66 at Different pHs. For the purpose of structural analyses, the degradation reaction of DMNP was scaled-up to 50 mg of UiO-66 in 43.75 mL of water and 6.25 mL of 8 mM DMNP, leading to a total volume of 50 mL and DMNP concentration of 1 mM at pH 3.8 (natural), 5.5, 7.0, 8.5, 9.5, and 11.0. The pH value was kept constant during the course of the reaction using the automatic titrator. After 1 h under stirring, solid UiO-66 was separated by centrifugation and DMNP, 4-NP, and terephthalic acid concentrations were measured using HPLC. Solid UiO-66 was washed three times with water and three times with acetone, air-dried for 24 h, and analyzed by XRD, SEM, and by nitrogen adsorption.

CONCLUSIONS

In previous reports, the potentiometric acid–base titration was suggested as a method for evaluation of acidity of protons of the $-\text{OH}_2$ and $-\text{OH}$ ligands, which compensate for missing terephthalate linkers.⁴⁵ Evaluation of the MOF acidity by the potentiometric titration would be valid only if the structure and composition of the titrated material would not change during the titration. Our quantitative analyses indicate that this assumption is not correct.

We summarize the results as follows: (i) A number of $-\text{OH}_2$ and $-\text{OH}$ ligands in unsaturated coordination sites of as-prepared UiO-66 are limited as these sites are verifiably occupied by modulator anions including formates generated *in situ* from DMF during the synthesis.^{20,43} (ii) In aqueous dispersions of UiO-66, coordinated acetates and formates released into water are responsible for its acidity (i.e., natural pH 3.8). It points to the importance of the washing procedure on the composition and properties of UiO-66. (iii) The release of the terephthalate linkers and monocarboxylate ligands during the titration evidently creates new defects (i.e., unsaturated coordination sites), not originally present in the structure (Scheme 1). This fact can be used for the intentional defect formation. (iv) Characterization methods generally used for quantification of MOF stabilities (SEM, XRD, and adsorption studies) are not conclusive. The subtle changes to the structure, indicated by released structural components, have to be analyzed by sensitive techniques such as HPLC. (v) New catalytic sites toward the dimethyl-4-nitrophenyl phosphate degradation are formed after the release of the linker or other compensating monocarboxylate ligands—the more massive release without the disruption of the structure, the higher catalytic activity of UiO-66. These results point to the dynamic nature of Zr-based MOFs where coordination/decoordination of ligands can occur at mild conditions and can significantly alter the resulting MOF properties. (vi) The leaching of terephthalate linker from UiO-66 shows that UiO-66 is not a good material for flow reactors in neutral and basic environments.

ASSOCIATED CONTENT

Supporting Information

The Supporting Information is available free of charge on the ACS Publications website at DOI: 10.1021/acs.inorgchem.8b02360.

Concentrations of released terephthalic, formic, and acetic acids from UiO-66 at different pHs, XRD patterns, SEM images, thermogravimetric analysis, ¹H NMR spectrum of dissolved UiO-66, nitrogen adsorption isotherms, kinetics of DMNP degradation and 4-NP formation, analysis of dimethyl phosphate formation (PDF)

AUTHOR INFORMATION

Corresponding Author

*E-mail: lang@iic.cas.cz.

ORCID

Daniel Bůžek: 0000-0002-7387-9461

Jan Demel: 0000-0001-7796-6338

Kamil Lang: 0000-0002-4151-8805

Notes

The authors declare no competing financial interest.

ACKNOWLEDGMENTS

The work was supported by the Czech Science Foundation (No. 16-02098S) and by the Student Grant Agency of the University of Jan Evangelista Purkyně in Ústí nad Labem. The authors acknowledge the assistance provided by the Research Infrastructure NanoEnvCz, supported by the Ministry of Education, Youth and Sports of the Czech Republic under Project No. LM2015073. We thank Petr Bezdička for XRD, Slavomír Adamec for ICP-MS, and Jan Hynek for NMR measurements.

REFERENCES

- Rowell, J. L. C.; Yaghi, O. M. Metal–Organic Frameworks: A New Class of Porous Materials. *Microporous Mesoporous Mater.* **2004**, *73*, 3–14.
- Férey, G. Hybrid Porous Solids: Past, Present, Future. *Chem. Soc. Rev.* **2008**, *37*, 191–214.
- Farha, O. K.; Eryazici, I.; Jeong, N. C.; Hauser, B. G.; Wilmer, Ch. E.; Sarjeant, A. A.; Snurr, R. Q.; Nguyen, S. T.; Yazaydin, A. Ö.; Hupp, J. T. Metal–Organic Framework Materials with Ultrahigh Surface Areas: Is the Sky the Limit? *J. Am. Chem. Soc.* **2012**, *134*, 15016–15021.
- Li, J.-R.; Sculley, J.; Zhou, H.-C. Metal–Organic Frameworks for Separations. *Chem. Rev.* **2012**, *112*, 869–932.
- He, Y.; Zhou, W.; Qian, G.; Chen, B. Methane Storage in Metal–Organic Frameworks. *Chem. Soc. Rev.* **2014**, *43*, 5657–5678.
- Corma, A.; García, H.; Llabrés i Xamena, F. X. Engineering Metal Organic Frameworks for Heterogeneous Catalysis. *Chem. Rev.* **2010**, *110*, 4606–4655.
- Tai, S.; Zhang, W.; Zhang, J.; Luo, G.; Jia, Y.; Deng, M.; Ling, Y. Facile Preparation of UiO-66 Nanoparticles with Tunable Sizes in a Continuous Flow Microreactor and its Application in Drug Delivery. *Microporous Mesoporous Mater.* **2016**, *220*, 148–154.
- Kreno, L. E.; Leong, K.; Farha, O. K.; Allendorf, M.; Van Duyne, R. P.; Hupp, J. T. Metal–Organic Framework Materials as Chemical Sensors. *Chem. Rev.* **2012**, *112*, 1105–1125.
- Dias, E. M.; Petit, C. Towards the Use of Metal–Organic Frameworks for Water Reuse: A Review of the Recent Advances in the Field of Organic Pollutants Removal and Degradation and the Next Steps in the Field. *J. Mater. Chem. A* **2015**, *3*, 22484–22506.
- Bobbitt, N. S.; Mendonca, M. L.; Howarth, A. J.; Islamoglu, T.; Hupp, J. T.; Farha, O. K.; Snurr, R. Q. Metal–Organic Frameworks for the Removal of Toxic Industrial Chemicals and Chemical Warfare Agents. *Chem. Soc. Rev.* **2017**, *46*, 3357–3385.
- Wang, J.-L.; Wang, Ch.; Lin, W. Metal–Organic Frameworks for Light Harvesting and Photocatalysis. *ACS Catal.* **2012**, *2*, 2630–2640.
- Wang, Ch.-Ch.; Du, X.-D.; Li, J.; Guo, X.-X.; Wang, P.; Zhang, J. Photocatalytic Cr(VI) Reduction in Metal–Organic Frameworks: A Mini-Review. *Appl. Catal., B* **2016**, *193*, 198–216.
- Howarth, A. J.; Liu, Y.; Li, P.; Li, Z.; Wang, T. C.; Hupp, J. T.; Farha, O. K. Chemical, Thermal and Mechanical Stabilities of Metal–Organic Frameworks. *Nat. Rev. Mater.* **2016**, *1*, 15018.
- Mondloch, J. E.; Katz, M. J.; Planas, N.; Semrouni, D.; Gagliardi, L.; Hupp, J. T.; Farha, O. K. Are Zr₆-based MOFs Water

Stable? Linker Hydrolysis vs. Capillary-Force-Driven Channel Collapse. *Chem. Commun.* **2014**, *50*, 8944–8946.

(15) DeCoste, J. B.; Peterson, G. W.; Jasuja, H.; Glover, T. G.; Huang, Y.-G.; Walton, K. S. Stability and Degradation Mechanisms of Metal–Organic Frameworks Containing the $Zr_6O_4(OH)_4$ Secondary Building Unit. *J. Mater. Chem. A* **2013**, *1*, 5642–5650.

(16) Cavka, J. H.; Jakobsen, S.; Olsbye, U.; Guillou, N.; Lamberti, C.; Bordiga, S.; Lillerud, K. P. A New Zirconium Inorganic Building Brick Forming Metal Organic Frameworks with Exceptional Stability. *J. Am. Chem. Soc.* **2008**, *130*, 13850–13851.

(17) Fang, Z.; Bueken, B.; De Vos, D. E.; Fischer, R. A. Defect-Engineered Metal–Organic Frameworks. *Angew. Chem., Int. Ed.* **2015**, *54*, 7234–7254.

(18) Valenzano, L.; Civalleri, B.; Chavan, S.; Bordiga, S.; Nilsen, M. H.; Jakobsen, S.; Lillerud, K. P.; Lamberti, C. Disclosing the Complex Structure of UiO-66 Metal Organic Framework: A Synergic Combination of Experiment and Theory. *Chem. Mater.* **2011**, *23*, 1700–1718.

(19) Wu, H.; Chua, Y. S.; Krungleviciute, V.; Tyagi, M.; Chen, P.; Yildirim, T.; Zhou, W. Unusual and Highly Tunable Missing-Linker Defects in Zirconium Metal–Organic Framework UiO-66 and Their Important Effects on Gas Adsorption. *J. Am. Chem. Soc.* **2013**, *135*, 10525–10532.

(20) Shearer, G. C.; Chavan, S.; Bordiga, S.; Svelle, S.; Olsbye, U.; Lillerud, K. P. Defect Engineering: Tuning the Porosity and Composition of the Metal–Organic Framework UiO-66 via Modulated Synthesis. *Chem. Mater.* **2016**, *28*, 3749–3761.

(21) Taddei, M. When Defects Turn into Virtues: The Curious Case of Zirconium-Based Metal–Organic Frameworks. *Coord. Chem. Rev.* **2017**, *343*, 1–24.

(22) Kamerlin, S. C. L.; Sharma, P. K.; Prasad, R. B.; Warshel, A. Why Nature Really Chose Phosphate. *Q. Rev. Biophys.* **2013**, *46*, 1–132.

(23) Eddleston, M.; Buckley, N. A.; Eyer, P.; Dawson, A. H. Management of Acute Organophosphorus Pesticide Poisoning. *Lancet* **2008**, *371*, 597–607.

(24) Sidell, F. R.; Borak, J. Chemical Warfare Agents: II. Nerve Agents. *Ann. Emerg. Med.* **1992**, *21*, 865–871.

(25) Kim, K.; Tsay, O. G.; Atwood, D. A.; Churchill, D. G. Destruction and Detection of Chemical Warfare Agents. *Chem. Rev.* **2011**, *111*, 5345–5403.

(26) Anzueto, A.; Delemos, R. A.; Seidenfeld, J.; Moore, G.; Hamil, H.; Johnson, D.; Jenkinson, S. G. Acute Inhalation Toxicity of Soman and Sarin in Baboons. *Toxicol. Sci.* **1990**, *14*, 676–687.

(27) Razzaque, M. S. Phosphate Toxicity: New Insights into an Old Problem. *Clin. Sci.* **2011**, *120*, 91–97.

(28) Pehkonen, S. O.; Zhang, Q. The Degradation of Organophosphorus Pesticides in Natural Waters: A Critical Review. *Crit. Rev. Environ. Sci. Technol.* **2002**, *32*, 17–72.

(29) Rodrigo, M. A.; Oturan, N.; Oturan, M. A. Electrochemically Assisted Remediation of Pesticides in Soils and Water: A Review. *Chem. Rev.* **2014**, *114*, 8720–8745.

(30) Sud, D.; Kaur, P. Heterogeneous Photocatalytic Degradation of Selected Organophosphate Pesticides: A Review. *Crit. Rev. Environ. Sci. Technol.* **2012**, *42*, 2365–2407.

(31) Yadav, M.; Shukla, A. K.; Srivastva, N.; Upadhyay, S. N.; Dubey, S. K. Utilization of Microbial Community Potential for Removal of Chlorpyrifos: A Review. *Crit. Rev. Biotechnol.* **2016**, *36*, 727–742.

(32) Janoš, P.; Henych, J.; Pelant, O.; Pilařová, V.; Vrtoch, L.; Kormunda, M.; Mazanec, K.; Štengl, V. Cerium Oxide for the Destruction of Chemical Warfare Agents: A Comparison of Synthetic Routes. *J. Hazard. Mater.* **2016**, *304*, 259–268.

(33) Wagner, G. W.; Peterson, G. W.; Mahle, J. J. Effect of Adsorbed Water and Surface Hydroxyls on the Hydrolysis of VX, GD, and HD on Titania Materials: The Development of Self-Decontaminating Paints. *Ind. Eng. Chem. Res.* **2012**, *51*, 3598–3603.

(34) Moon, S. Y.; Liu, Y.; Hupp, J. T.; Farha, O. K. Instantaneous Hydrolysis of Nerve-Agent Simulants with a Six-Connected

Zirconium-Based Metal–Organic Framework. *Angew. Chem., Int. Ed.* **2015**, *54*, 6795–6799.

(35) Li, P.; Klet, R. C.; Moon, S. Y.; Wang, T. C.; Deria, P.; Peters, A. W.; Klahr, B. M.; Park, H. J.; Al-Juaid, S. S.; Hupp, J. T.; Farha, O. K. Synthesis of Nanocrystals of Zr-based Metal–Organic Frameworks with csq-net: Significant Enhancement in the Degradation of a Nerve Agent Simulant. *Chem. Commun.* **2015**, *51*, 10925–10928.

(36) Katz, M. J.; Moon, S. Y.; Mondloch, J. E.; Beyzavi, M. H.; Stephenson, C. J.; Hupp, J. T.; Farha, O. K. Exploiting Parameter Space in MOFs: a 20-fold Enhancement of Phosphate-ester Hydrolysis with UiO-66-NH₂. *Chem. Sci.* **2015**, *6*, 2286–2291.

(37) Peterson, G. W.; Moon, S. Y.; Wagner, G. W.; Hall, M. G.; DeCoste, J. B.; Hupp, J. T.; Farha, O. K. Tailoring the Pore Size and Functionality of UiO-Type Metal–Organic Frameworks for Optimal Nerve Agent Destruction. *Inorg. Chem.* **2015**, *54*, 9684–9686.

(38) Mondal, S. S.; Holdt, H. J. Breaking Down Chemical Weapons by Metal–Organic Frameworks. *Angew. Chem., Int. Ed.* **2016**, *55*, 42–44.

(39) Nunes, P.; Gomes, A. C.; Pillinger, M.; Goncalves, I. S.; Abrantes, M. Promotion of Phosphoester Hydrolysis by the Zr^{IV}-based Metal–Organic Framework UiO-67. *Microporous Mesoporous Mater.* **2015**, *208*, 21–29.

(40) Katz, M. J.; Mondloch, J. E.; Totten, R. K.; Park, J. K.; Nguyen, S. T.; Hupp, J. T.; Farha, O. K. Simple and Compelling Biomimetic Metal–Organic Framework Catalyst for the Degradation of Nerve Agent Simulants. *Angew. Chem., Int. Ed.* **2014**, *53*, 497–501.

(41) Katz, M. J.; Klet, R. C.; Moon, S. Y.; Mondloch, J. E.; Hupp, J. T.; Farha, O. K. One Step Backward Is Two Steps Forward: Enhancing the Hydrolysis Rate of UiO-66 by Decreasing [OH⁻]. *ACS Catal.* **2015**, *5*, 4637–4642.

(42) Gutov, O. V.; Hevia, M. G.; Escudero-Adán, E. C.; Shafir, A. Metal–Organic Framework (MOF) Defects under Control: Insights into the Missing Linker Sites and Their Implication in the Reactivity of Zirconium-Based Frameworks. *Inorg. Chem.* **2015**, *54*, 8396–8400.

(43) Taddei, M.; Wakeham, R. J.; Koutsianos, A.; Andreoli, E.; Barron, A. R. Post-Synthetic Ligand Exchange in Zirconium-Based Metal–Organic Frameworks: Beware of the Defects! *Angew. Chem., Int. Ed.* **2018**, *57*, 11706–11710.

(44) Shearer, G. C.; Chavan, S.; Ethiraj, J.; Vitillo, J. G.; Svelle, S.; Olsbye, U.; Lamberti, C.; Bordiga, S.; Lillerud, K. P. Tuned to Perfection: Ironing Out the Defects in Metal–Organic Framework UiO-66. *Chem. Mater.* **2014**, *26*, 4068–4071.

(45) Klet, R. C.; Liu, Y.; Wang, T. C.; Hupp, J. T.; Farha, O. K. Evaluation of Bronsted Acidity and Proton Topology in Zr- and Hf-Based Metal–Organic Frameworks Using Potentiometric Acid–Base Titration. *J. Mater. Chem. A* **2016**, *4*, 1479–1485.

(46) Bandosz, T. J.; Laskoski, M.; Mahle, J.; Mogilevsky, G.; Peterson, G. W.; Rossin, J. A.; Wagner, G. W. Reactions of VX, GD, and HD with Zr(OH)₄: Near Instantaneous Decontamination of VX. *J. Phys. Chem. C* **2012**, *116*, 11606–11614.

(47) JCPDS PDF-2 database, release 54, International Centre for Diffraction Data: Newtown Square, PA, USA, 2004.